

## Three-dimensional structure and evolution of stratospheric $\text{HNO}_3$ based on UARS Microwave Limb Sounder measurements

M. L. Santee,<sup>1</sup> G. L. Manney,<sup>1,2</sup> N. J. Livesey,<sup>1</sup> and W. G. Read<sup>1</sup>

**Abstract.** The UARS Microwave Limb Sounder (MLS) measured the global distribution of stratospheric  $\text{HNO}_3$  through more than seven complete annual cycles in both hemispheres. Here we present an overview of the seasonal, interhemispheric, and interannual variations in the distribution of  $\text{HNO}_3$  throughout the lower and middle stratosphere from 420 to 960 K potential temperature based on the UARS MLS version 6  $\text{HNO}_3$  measurements. The version 6 MLS data have much better precision and a larger vertical range than previous MLS  $\text{HNO}_3$  datasets, and have also been corrected to account for an oversight in the retrieval algorithms that led earlier versions to overestimate  $\text{HNO}_3$  abundances by as much as 35% at some levels in the stratosphere.  $\text{HNO}_3$  exhibits little vertical, seasonal, or interannual variability in the tropics. For the first  $\sim 1.5$  years of the mission, however, a persistent enhancement is seen at low and midlatitudes that we attribute to perturbations in reactive nitrogen chemistry under conditions of high aerosol loading from the eruption of Mount Pinatubo. The signature of Pinatubo-induced  $\text{HNO}_3$  enhancement is considerably weaker at 420 and 465 K than at higher altitudes, and at northern middle and high latitudes than in the southern hemisphere.  $\text{HNO}_3$  abundances increase towards the pole in both hemispheres at all levels and in all seasons, with the exception of the severely-denitrified region inside the Antarctic vortex. A pronounced seasonal cycle is present at middle and high latitudes up to at least 960 K ( $\sim 34$  km), with a winter maximum and a summer minimum. Large interannual variability in the timing, magnitude, and duration of enhanced wintertime  $\text{HNO}_3$  abundances is seen in both hemispheres. Even in the coldest Arctic winters,  $\text{HNO}_3$  depletion is modest and limited in both horizontal and vertical extent. In contrast, virtually complete removal of gas-phase  $\text{HNO}_3$  occurs at the highest southern latitudes by July in every year throughout the lower stratosphere. Indications of denitrification are present up to at least 740 K, well above the highest altitude at which dehydration is observed, providing further evidence that denitrification can proceed in the absence of dehydration.

### 1. Introduction

Nitric acid ( $\text{HNO}_3$ ) plays several pivotal roles in the processes controlling stratospheric ozone depletion [e.g., Solomon, 1999; World Meteorological Organization, 2003]. Over the past few decades,  $\text{HNO}_3$  has been measured by a variety of ground-based, aircraft, balloon, and satellite in-

struments [see Santee *et al.*, 1999, and references therein, for a brief review]. By far the most complete observational record to date has been obtained by the Microwave Limb Sounder (MLS) onboard the Upper Atmosphere Research Satellite (UARS), which measured the global distribution of stratospheric  $\text{HNO}_3$  over annual cycles for much of the 1990s, albeit with reduced sampling frequency in the latter half of the decade. The UARS MLS  $\text{HNO}_3$  dataset, unique in its scope, was previously examined by Santee *et al.* [1999]

<sup>1</sup>Jet Propulsion Laboratory, California Institute of Technology, Pasadena.

<sup>2</sup>Department of Natural Sciences, New Mexico Highlands University.

to explore the seasonal, interhemispheric, and interannual variations in the distribution of  $\text{HNO}_3$ . Although important conclusions were drawn from this study, it suffered from a number of limitations: It was confined to a single level in the lower stratosphere (465 K potential temperature,  $\sim 19$  km altitude), it was based on version 4 MLS data, and it relied heavily on zonal-mean comparisons of the evolution of  $\text{HNO}_3$  in the northern and southern hemispheres. Here we update and significantly expand the previous work by examining the distribution of  $\text{HNO}_3$  throughout the lower and middle stratosphere from 420 to 960 K. We use version 6 MLS  $\text{HNO}_3$  data, which, in addition to having much better precision, a larger vertical range, and better definition of the  $\text{HNO}_3$  profile, have also been corrected to account for the neglect of some excited vibrational state lines that caused the version 4 (and version 5) retrievals to substantially overestimate  $\text{HNO}_3$  peak values [Livesey *et al.*, 2003]. In addition, we calculate averages over equivalent latitude (the latitude that would enclose the same area between it and the pole as a given contour of potential vorticity [Butchart and Remsberg, 1986]); such averages give a much more representative view of the behavior of  $\text{HNO}_3$  in the context of the stratospheric flow and vortex evolution than zonal means, especially in the Arctic winter.

In the next section we briefly review the UARS MLS data coverage and summarize the quality of the version 6  $\text{HNO}_3$  measurements. We then examine time series of different slices through the data to develop a comprehensive picture of the mean evolution of stratospheric  $\text{HNO}_3$  during the UARS timeframe. Seasonal “snapshots” — maps and equivalent latitude/potential temperature cross sections — are shown to illustrate the typical behavior of  $\text{HNO}_3$  during several intervals of particular interest in the annual cycle. Climatological fields are derived by averaging together the results for individual years. The climatologies presented here provide a valuable baseline for comparison with observations expected from NASA’s upcoming Earth Observing System (EOS) Aura mission. Aura will carry several instruments capable of measuring  $\text{HNO}_3$  in the stratosphere, including a second-generation MLS experiment. The improvements over UARS anticipated in the Aura MLS  $\text{HNO}_3$  measurements are discussed in the last section.

## 2. MLS $\text{HNO}_3$ Data Coverage and Quality

Microwave limb sounding and the UARS MLS instrument are described by, for example, Waters [1993], Barath *et al.* [1993], and Waters *et al.* [1999]. Latitudinal coverage of the MLS measurements extended from  $80^\circ$  on one side of the equator to  $34^\circ$  on the other. Approximately 10 times per year UARS performed a  $180^\circ$  yaw maneuver such

that MLS alternated between viewing northern and southern high latitudes, with the first day of a given UARS yaw period occurring  $\sim 5$  days earlier each year. As a consequence, on a particular day of the year MLS may have been viewing northern high latitudes in some years but southern high latitudes in others. A calendar of MLS daily data coverage and a detailed chronology of MLS operations are provided by Livesey *et al.* [2003] (see also section 2.1 of Santee *et al.* [1999]). After several years in orbit, degradation in the performance of the MLS antenna scan mechanism, together with a reduction in power available from the UARS spacecraft, resulted in markedly reduced data sampling. The relative sparsity of the data collected after 1998 limits their utility in establishing a climatology of this kind, and they are not included here.

A full description of the MLS version 5 (v5) retrieval algorithms and resulting dataset is given by Livesey *et al.* [2003]. Here we very briefly describe the major changes in the algorithms and their impact on the  $\text{HNO}_3$  retrievals. The most significant change is that in v5 geophysical parameters are retrieved on every UARS surface (six surfaces per decade change in pressure, as opposed to three in previous MLS datasets). The v5 retrievals thus allow better definition of the  $\text{HNO}_3$  profile. The inherent vertical resolution of the instrument is coarser than the v5 retrieval grid, however. Furthermore, vertical smoothing is applied to enhance retrieval stability. As a consequence, the true vertical resolution of the v5  $\text{HNO}_3$  data (which varies with altitude from 4.5 km at 100 hPa to 10.5 km at 4.6 hPa) is approximately the same as, and the v5 profiles are generally smoother than, the previous version. Along with the smoothing, more rigorous error propagation as well as improvements in the ozone (retrieved in the same band as  $\text{HNO}_3$ ) and tangent pressure retrievals have led to substantially better (by a factor of 2–3)  $\text{HNO}_3$  precision in v5 than in v4, even though the v5 retrievals are performed on every UARS surface; the single-profile precision is now  $\sim 1.0$ – $1.5$  ppbv throughout the vertical range. In addition, inclusion in the retrievals of the emission from several weak  $\text{HNO}_3$  lines in the bands primarily used to measure ClO has provided information at higher altitudes and has extended the vertical range for reliable measurements up to 4.6 hPa (from 22 hPa in v4). Finally, strong negative biases (2–3 ppbv over a broad area) in the equatorial regions at 22 and 46 hPa present in the v4  $\text{HNO}_3$  data have been eliminated in this version.

After the MLS v5 data reprocessing was completed, it was discovered that neglecting emission from  $\text{HNO}_3$   $v_9$  and  $v_7$  excited vibrational states caused v5 (and v4) values to significantly overestimate  $\text{HNO}_3$  abundances at some levels in the stratosphere. An empirical correction to the MLS v5  $\text{HNO}_3$  dataset has been derived and is described in detail

by Livesey *et al.* [2003]. The correction is a linear, strongly temperature-dependent scaling that leads to reductions in the reported v5  $\text{HNO}_3$  mixing ratios of about 4–8% at 100 hPa, 10–20% at 32 hPa, and 25–35% at 10 hPa, depending on the latitude and season. The corrected MLS  $\text{HNO}_3$  dataset is referred to as “v6”. The v6  $\text{HNO}_3$  data are available from the NASA Goddard Space Flight Center Distributed Active Archive Center (GSFC DAAC).

Livesey *et al.* [2003] summarize comparisons of MLS v6  $\text{HNO}_3$  with other  $\text{HNO}_3$  datasets, including those from the UARS Cryogenic Limb Array Etalon Spectrometer (CLAES), the Atmospheric Trace Molecule Spectroscopy (ATMOS) experiment, the Improved Limb Atmospheric Spectrometer (ILAS) [see also Danilin *et al.*, 2002], and the Ground-based Millimeter-wave Spectrometer (GBMS) [see also Muscari *et al.*, 2002]. Although comparisons between MLS and these other instruments do not always provide a consistent picture, they suggest that the following artifacts are present in the MLS v6  $\text{HNO}_3$  data: (1) a high bias of as much as  $\sim 2$ – $3$  ppbv in the equatorial regions during the first  $\sim 100$  days of the mission, caused by enhanced stratospheric  $\text{SO}_2$  (which is not retrieved as part of the v5 data processing) from the eruption of Mount Pinatubo, (2) a high bias of as much as 3–5 ppbv during Antarctic late winter at 585 and 620 K (with a smaller effect at 520 K), arising from nonlinearities with respect to temperature in the MLS retrieval system, and (3) a low bias of  $\sim 1$ – $3$  ppbv at the topmost levels (above 740 K,  $\sim 10$ – $15$  hPa). Based on the comparisons reported by Livesey *et al.* [2003], the MLS v6  $\text{HNO}_3$  data are expected to be accurate to within  $\sim 3$  ppbv above  $\sim 15$  hPa and  $\sim 2$  ppbv below, except in the lower stratospheric winter polar vortices, where biases may be slightly larger.

### 3. $\text{HNO}_3$ Climatology from UARS MLS

#### 3.1. Equivalent Latitude Time Series

We begin by showing a time series to track the mean evolution of stratospheric  $\text{HNO}_3$  over seven annual cycles in both hemispheres. The averages shown in Figure 1 are similar to zonal means, but they have been calculated as a function of potential vorticity (PV) expressed in terms of equivalent latitude (EqL, [Butchart and Remsberg, 1986]), rather than geographic latitude. The data have been interpolated to the 585 K potential temperature ( $\theta$ ) surface, near the peak in the  $\text{HNO}_3$  profile. The temperatures used for the interpolation to  $\theta$  surfaces are taken from the U.K. Met Office analyses [Swinbank and O'Neill, 1994]; PV is also calculated from Met Office fields. For clarity of presentation, small data gaps of a few days or less have been filled in this plot by running the daily averages through a Kalman smoother. Blank spaces appear where the error in the in-

terpolated values exceeds a certain threshold, indicating that the interval is too far from actual measurements. This plot clearly illustrates the interruption in MLS high-latitude data coverage arising from the regular UARS yaw maneuvers, the long data gap stretching from October 1994 through July 1995 caused by problems with the MLS scan system and the UARS batteries and solar array, and the generally decreasing MLS measurement frequency as the mission progressed.

Many aspects of the stratospheric distribution of  $\text{HNO}_3$  are evident in Figure 1. For example,  $\text{HNO}_3$  abundances increase from low to high equivalent latitudes in both hemispheres and in all seasons, with the exception of the regions of strong polar stratospheric cloud (PSC) formation and denitrification in the southern hemisphere winter polar vortex (discussed further below). In addition, a pronounced seasonal cycle is evident at higher EqLs in both hemispheres, with a winter maximum and a summer minimum, whereas the seasonal cycle at lower latitudes is weak or nonexistent. Both the latitudinal and the seasonal variations in  $\text{HNO}_3$  have been noted in numerous previous studies [e.g., Santée *et al.*, 1999, and references therein].

Figure 1 provides a qualitative sense of the repeatability of the seasonal changes from year to year and the inter-hemispheric differences in the magnitude of those changes. At this level and below, wintertime  $\text{HNO}_3$  mixing ratios are primarily controlled by meteorological conditions: the strength of the diabatic descent, the permeability of the vortex, and the spatial extent and duration of low temperatures (which govern PSC formation). The northern and southern hemispheres are characterized by distinctly different seasonal temperature patterns and vortex behavior. In the Arctic, lower stratospheric winter temperatures are  $\sim 15$ – $20$  K higher, on average, and the vortex is smaller, weaker, more distorted, more variable, and shorter-lived than in the Antarctic [e.g., Andrews, 1989; Waugh and Randel, 1999; Waugh *et al.*, 1999]. Whereas in the south temperatures in the lower stratospheric vortex tend to exhibit a more or less steady decline beginning in autumn to (and below) the thresholds for PSC formation, in the north greater dynamical activity is accompanied by rapid temperature variations. In general these conditions lead to fewer, less persistent PSC events in the Arctic [e.g., Poole and Pitts, 1994; Fromm *et al.*, 1999]. During the mid-1990s when the bulk of the UARS MLS  $\text{HNO}_3$  measurements were made, however, the Arctic lower stratospheric vortex was unusually strong and long-lived [Waugh *et al.*, 1999], less variable from year to year, and atypically cold, with prolonged periods of temperatures low enough for extensive PSC formation [e.g., Zurek *et al.*, 1996; Pawson and Naujokat, 1999]. Nevertheless, the episodes of PSC activity in the Arctic were sufficiently localized and transient at this level in all of these years that none

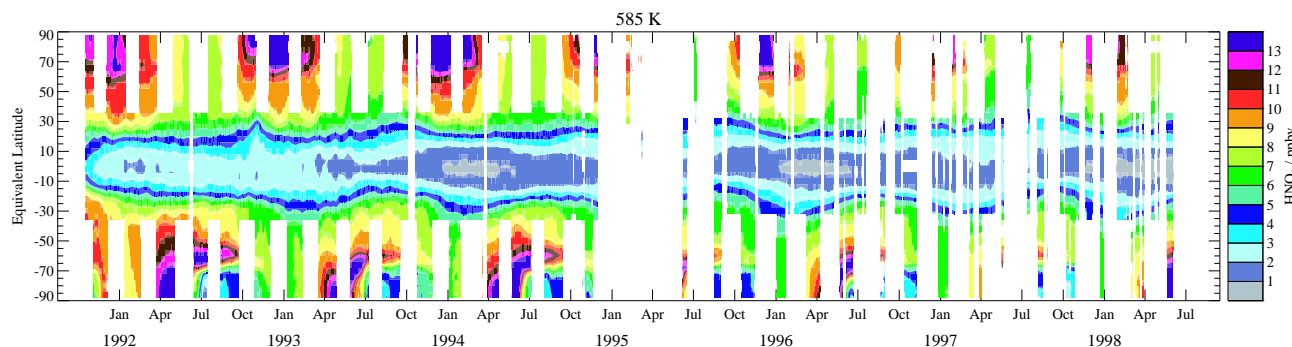


**Figure 1.** Time series over seven years of MLS v6  $\text{HNO}_3$  at 585 K as a function of equivalent latitude (EqL). Small data gaps have been filled by running the daily vortex averages through a Kalman smoother (see text).

are discernible in the daily EqL averages shown here (though they are clearly visible in daily  $\text{HNO}_3$  maps [e.g., Santee *et al.*, 1996, 1997, 1999]). In contrast, widespread PSC formation and denitrification are observed in the Antarctic in every year. (Note that since MLS is sensitive only to gas-phase  $\text{HNO}_3$ , MLS measurements alone cannot be used to distinguish temporary  $\text{HNO}_3$  sequestration in PSCs from permanent denitrification, the removal of reactive nitrogen from the stratosphere through the sedimentation of PSCs; however, the occurrence of denitrification can be inferred from the persistent depression in gas-phase  $\text{HNO}_3$  concentrations in November, well after the stratosphere has warmed above PSC existence thresholds [Santee *et al.*, 1995, 1999].)

As noted earlier, low latitudes exhibit negligible  $\text{HNO}_3$  seasonal variation. Figure 1 does, however, suggest that  $\text{HNO}_3$  abundances at low EqLs are slightly elevated for the first  $\sim 1.5$  years of the mission. One caveat in interpreting this plot is the  $\sim 2\text{--}3$  ppbv high bias present in individual MLS  $\text{HNO}_3$  measurements in the equatorial regions for the first  $\sim 100$  days, an artifact induced by enhanced stratospheric  $\text{SO}_2$  from the eruption of Mount Pinatubo (section 2, see also Livesey *et al.* [2003]). The residual  $\text{SO}_2$  from Pinatubo was almost entirely confined to the latitude band between  $30^\circ\text{S}$  and  $15^\circ\text{N}$  at this time [Read *et al.*, 1993] and did not affect midlatitude MLS  $\text{HNO}_3$  retrievals. We attribute the persistent enhancement in  $\text{HNO}_3$  at midlatitudes, and at low latitudes after the first few months, to the heterogeneous hydrolysis of  $\text{N}_2\text{O}_5$  on volcanic aerosol [e.g., Hofmann and Solomon, 1989; Brasseur and Granier, 1992; Webster *et al.*, 1994; Rinsland *et al.*, 1994, 2003], with the decline in  $\text{HNO}_3$  values after mid-1993 resulting from the decay of this aerosol [e.g., Thomason *et al.*, 1997; Bauman *et al.*, 2003]. Gradual recovery from Pinatubo-induced  $\text{HNO}_3$  enhancement has also been seen in ground-based column amounts [e.g., Koike *et al.*, 1994; David *et al.*, 1994; Slusser *et al.*, 1998; Rinsland *et al.*, 2003] and UARS CLAES  $\text{HNO}_3$  measurements [Kumer *et al.*, 1996], and

trends in MLS  $\text{HNO}_3$  data have also been discussed by Randel *et al.* [1999].

The enhancement in  $\text{HNO}_3$  in the early part of the mission is washed out when seven years of data are averaged together to produce climatological fields, as shown in Figure 2. Climatological time series are shown for eight  $\theta$  surfaces close to the standard UARS pressure levels used for the MLS v5 retrievals; it should be noted, however, that because of the vertical resolution of the data, the  $\text{HNO}_3$  values obtained at these levels are not completely independent. Because a given UARS yaw period starts about 5 days earlier in each succeeding year, the data gaps visible in Figure 1 are shortened when several years of measurements are averaged together. Averaging does not remove the gaps entirely, however, so to eliminate breaks in the climatological fields, Kalman smoothing has been applied to the averaged  $\text{HNO}_3$  values at each level. Unlike in Figure 1, where intervals far from actual measurements were blanked out, in the climatologies shown in Figure 2, the regions in which the estimated precision of the interpolated values is poor are denoted by paler colors. In order to ensure that one anomalous day/year does not dominate the climatological fields, a greater degree of smoothing has been applied to these averages than was used in Figure 1. Nevertheless, “edge effects” are still evident near the UARS yaw period boundaries, where data from only one or two years may contribute to the average; these effects are particularly pronounced in the lower stratosphere, where interannual variability strongly influences  $\text{HNO}_3$  abundances.

Figure 2 shows that weak seasonal patterns are present in  $\text{HNO}_3$  at middle and high latitudes up to at least 960 K ( $\sim 34$  km). Microphysical model calculations [e.g., Mills *et al.*, 1999; de Zafra and Smyshlyaev, 2001] have indicated that the formation of small sulfate particles can lead to enhanced aerosol surface area in the winter polar regions up to or even slightly above 35 km. Conversion of  $\text{NO}_2$  into  $\text{N}_2\text{O}_5$

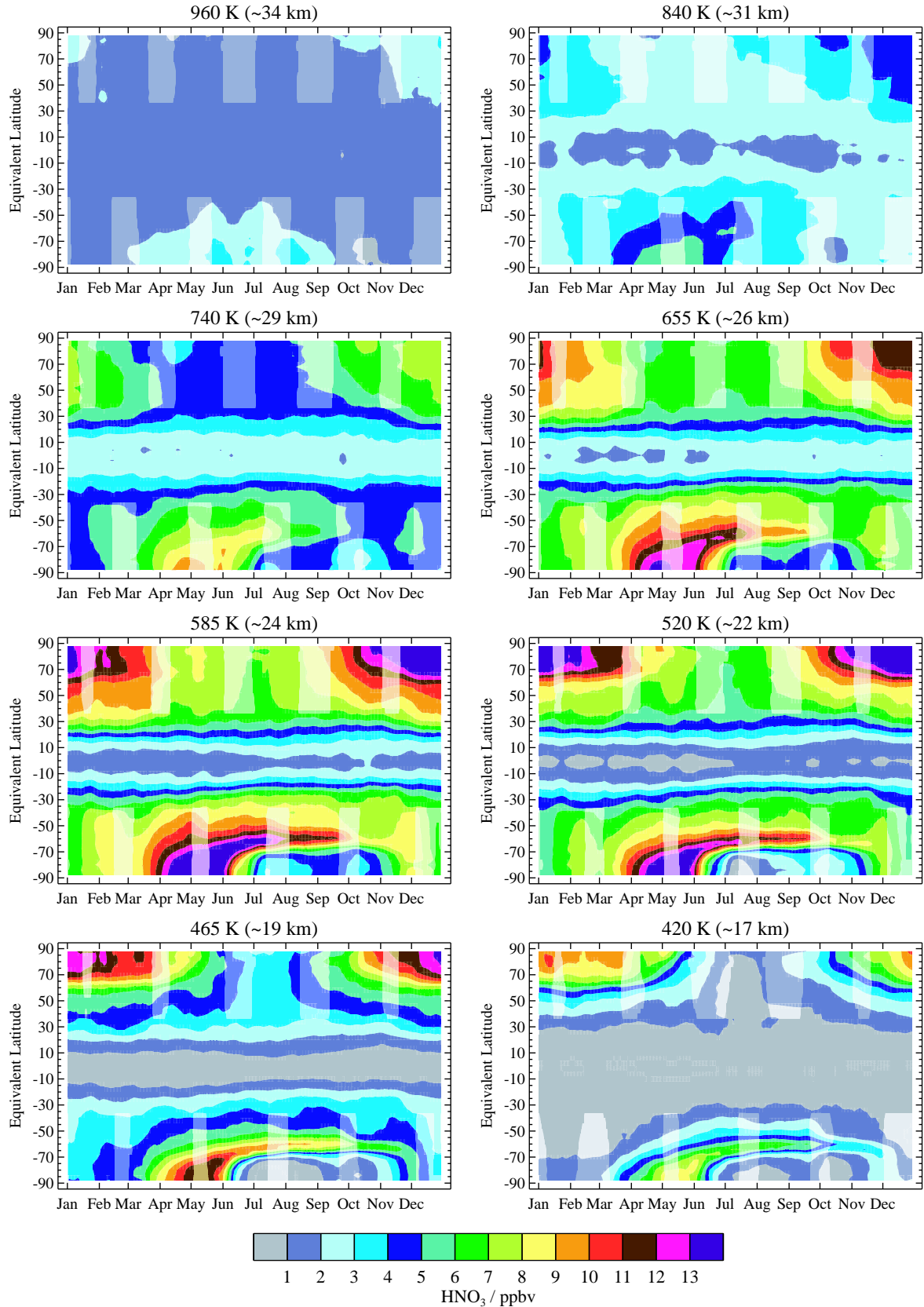


**Figure 2.** Climatologies of MLS v6  $\text{HNO}_3$  as a function of EqL and time at eight potential temperature levels between 960 and 420 K, derived by averaging together the results for seven individual years at each level. To fill in breaks in the climatological fields arising from data gaps, Kalman smoothing has been applied to the averaged  $\text{HNO}_3$  values at each level; paler colors denote regions where the estimated precision of the interpolated values is poor.

followed by heterogeneous hydrolysis of  $\text{N}_2\text{O}_5$  to  $\text{HNO}_3$  on sulfate aerosols [e.g., Austin et al., 1986], coupled with the cessation during polar night of  $\text{HNO}_3$  loss through photolysis and reaction with OH, leads to wintertime increases in  $\text{HNO}_3$  throughout the lower and middle stratospheric vortex [see, e.g., McDonald et al., 2000, for a more detailed discussion]. A broad peak in the high-latitude  $\text{HNO}_3$  profile is centered around 585 K, where mixing ratios in the two hemispheres are comparable. Maximum abundances at higher levels (655–960 K) are larger in the Antarctic than in the Arctic. This may reflect the fact that  $\text{NO}_2$  abundances at these levels are frequently higher in the south than in the north [Siskind et al., 1997; Randall et al., 1998; Rinsland et al., 1999], and/or that descent rates in the north are typically faster than those in the south throughout the winter [e.g., Manney et al., 1994], bringing down more air with lower  $\text{HNO}_3$  abundances to these levels. By the same token, more vigorous descent promotes maximum mixing ratios at the lowest levels (below the peak) that are larger in the north. Extensive and persistent PSC activity also acts to reduce  $\text{HNO}_3$  abundances throughout the Antarctic vortex core, where the signature of  $\text{HNO}_3$  depletion is seen over the range from 420 to 840 K. Maximum abundances are reached at all levels in the north in midwinter (December or early January), whereas PSC formation and denitrification start to reverse the seasonal increase in  $\text{HNO}_3$  in the south in early winter (May). Minimum temperatures are lower in the Antarctic vortex core than they are near the edge, leaving a band of higher  $\text{HNO}_3$  along the vortex rim (the so-called “collar” region [Toon et al., 1989]). Nevertheless, temperatures low enough to trigger significant growth of large PSC particles do extend into the vortex edge region, and it is likely that some degree of local denitrification takes place there. In addition, although large-scale mixing between the vortex core and edge regions is limited in the Antarctic until late winter/spring [e.g., Schoeberl et al., 1992; Bowman, 1993; Lee et al., 2001], transport of severely denitrified air from the vortex interior may lead to some dilution of  $\text{HNO}_3$  values in the collar region.

Figure 3 also shows time series of MLS  $\text{HNO}_3$  both for individual years and averaged together to produce climatological fields, but in this case the data have been averaged over the area encompassed by a certain EqL contour and displayed as a function of potential temperature. In other words, the values in Figure 3 are akin to vortex averages, except that they have been calculated over a fixed areal extent, rather than within a fixed PV contour, and are thus more relevant during the late spring and summer seasons when the area within a given PV contour may shrink substantially or even disappear. Unlike zonal means calculated over geographic latitude, however, they do not merge  $\text{HNO}_3$  abun-

dances measured inside and outside the winter vortex. To more closely approximate a vortex average when  $\text{HNO}_3$  is enhanced in winter, different EqL contours have been used to define the averages in the two hemispheres; in the north, the  $65^\circ$  EqL contour is situated in the region of strong PV gradients defining the winter vortex edge throughout the vertical domain considered here, whereas in the south the  $60^\circ$  EqL contour provides a similar relationship to the vortex edge.

The influence of diabatic descent is clearly seen in the downward tilt of the  $\text{HNO}_3$  contours in Figure 3, especially at higher altitudes. Although the Antarctic polar vortex starts to develop in the midstratosphere in March/April [e.g., Manney and Zurek, 1993; Waugh and Randel, 1999], the effects of confined descent are not immediately evident at these levels. Figure 3 shows that  $\text{HNO}_3$  mixing ratios at the upper levels remain relatively constant or even increase slightly through mid to late June, with a steep downward trend in the  $\text{HNO}_3$  contours appearing only in late June or July. Similar behavior has been observed around 30 km in GBMS  $\text{HNO}_3$  measurements obtained from South Pole Station [de Zafra et al., 1997; McDonald et al., 2000]; de Zafra et al. [1997] attribute the delay in the downturn in the  $\text{HNO}_3$  isopleths to the continuing conversion of  $\text{NO}_2$  into  $\text{HNO}_3$  as air descends from higher altitudes, with the direct effects of downward transport eventually becoming dominant. Dilution of the air brought down from above through mixing with air that has not experienced descent may also play a role in early fall, before the establishment of a strong transport barrier along the vortex edge. A corresponding evolution of the  $\text{HNO}_3$  contours occurs in the northern hemisphere. In contrast to the Antarctic lower stratosphere, where it becomes obscured by the onset of denitrification, in the Arctic a clear signature of descent is apparent throughout the winter over the entire altitude range.

A few other aspects of Figure 3 are worth noting. Although we have tried to minimize the influence of any particular year by applying slightly stronger smoothing in calculating the overall averages (as discussed in connection with Figure 2), it is clear that the anomalously high values of  $\text{HNO}_3$  measured in late spring and summer 1991/1992 have skewed the southern hemisphere climatological field. As will be discussed further below, the  $\text{HNO}_3$  enhancement during the first months of MLS measurements most likely arises from heterogeneous processing on volcanic aerosols in the wake of the Mount Pinatubo eruption the previous June. In addition, we note that in some years a sharp increase in  $\text{HNO}_3$  abundances occurs at the highest levels (above 900 K) in midwinter (e.g., late December 1992 in the north, late June 1993 in the south). This feature, which shows up weakly in the climatologies, probably represents the bottom end of the significant midwinter  $\text{HNO}_3$  enhancement

observed over the  $\sim 35$ – $50$  km altitude range in GBMS data [de Zafra et al., 1997, 2003; McDonald et al., 2000; de Zafra and Smyshlyaev, 2001] and also in UARS CLAES [Kawa et al., 1995] and Limb Infrared Monitor of the Stratosphere (LIMS) [Austin et al., 1986] data. de Zafra and Smyshlyaev [2001] show that this enhancement can be successfully modelled by heterogeneous reactions on sulfate aerosols below  $\sim 37$  km supplemented by ion cluster chemistry extending to  $\sim 45$ – $50$  km when a sufficiently large downward flux of  $\text{NO}_2$  from the polar winter mesosphere is included.

To take a more quantitative look at interannual and interhemispheric differences in the  $\text{HNO}_3$  seasonal cycle, the data are binned into  $5^\circ$  EqL bands and averaged; results are shown in Figure 4 for seven years at 585 K in 10 EqL bands in both hemispheres. A similar plot showing zonal mean values calculated over geographic latitude was presented for the 465 K level by Santee et al. [1999]. As discussed in that paper, only a faint seasonal cycle ( $\sim 2$  ppbv or less) is present at the lowest latitudes, where interannual variability and interhemispheric differences are also minimal. The magnitude of variability, both day-to-day and year-to-year, increases with increasing EqL and is quite considerable in the winter vortex core in both hemispheres.

The large disparity in the seasonal progression of vortex  $\text{HNO}_3$  in the two hemispheres is readily seen in Figure 4. In the fall, Antarctic  $\text{HNO}_3$  abundances at the highest EqLs exceed those in the Arctic by as much as 2 ppbv, as the developing vortex deepens more rapidly in the south [Manney and Zurek, 1993; Waugh and Randel, 1999] and provides a stronger barrier to mixing, allowing the effects of confined descent to raise  $\text{HNO}_3$  concentrations at this level. By early June, however, a steep decreasing trend becomes apparent in the south in every year, and the  $\text{HNO}_3$  abundances in the two hemispheres begin to depart substantially. Virtually complete removal of gas-phase  $\text{HNO}_3$  occurs at the highest southern EqLs in July from 420 to 840 K (not shown). (Note that the MLS retrieval algorithms occasionally produce negative mixing ratios, especially for noisy retrievals such as  $\text{HNO}_3$  when values are very low; though unphysical, these have been retained in order to avoid introducing biases into the averages.) Because of UARS yaw maneuvers and other data gaps, the maximum  $\text{HNO}_3$  mixing ratios attained in May were never captured in the MLS dataset, but PSC formation and denitrification are estimated to decrease the daily-average  $\text{HNO}_3$  values by more than 16 ppbv at 585 and 520 K in some years, and as much as 6 ppbv at 840 K. (Because of the progressively worse vertical resolution of the MLS  $\text{HNO}_3$  data with altitude, however, values at the topmost levels may be significantly influenced by those at lower levels.) In contrast, even in the coldest Arctic winters (e.g., 1995/1996, 1996/1997)  $\text{HNO}_3$  depletion of at

most 10–12 ppbv is seen in the daily averages in February from 420 to 585 K, the highest level at which a PSC-related decline in  $\text{HNO}_3$  values can be discerned in the north. In keeping with the smaller size of the Arctic vortex [Waugh and Randel, 1999],  $\text{HNO}_3$  depletion is also more limited geographically in the north, extending no further than  $70$ – $75^\circ$  EqL even at 465 K, whereas in the south it occurs into the  $65$ – $70^\circ$  EqL band, albeit less dramatically than at higher EqLs. Of course, it must be borne in mind that the inferences drawn from Figure 4 are based on averages taken over EqL bands, and that  $\text{HNO}_3$  removal processes may be operating on spatial scales not detectable in these averages (or indeed in the MLS data at all).

In the Antarctic,  $\text{HNO}_3$  concentrations at 585 K have begun to rebound by the beginning of the south-viewing observation period in early to mid-August, and they continue to increase through the November observation period.  $\text{HNO}_3$  is so severely depleted inside the Antarctic vortex at this level that mixing with lower latitude air as the vortex erodes in late spring causes the mixing ratios to rise at the highest EqLs. Evaporation of remaining PSCs may also play a role in the springtime  $\text{HNO}_3$  increase. In contrast, Arctic  $\text{HNO}_3$  decreases fairly steadily from March to May, through a combination of the effects of mixing after vortex breakdown and, after sunrise, photolysis. Note that averaging over EqL may obscure to some extent the effects of photolysis in the spring, especially in the northern hemisphere where the EqL contours are often not well-aligned with geographic latitude. Mixing ratios in both hemispheres level off at comparable summertime values in January/July. Based on the result that zonal-mean  $\text{HNO}_3$  values at 465 K for the two hemispheres are virtually indistinguishable at latitudes equatorward of  $\sim 65^\circ$ , even during winter, and that high-latitude  $\text{HNO}_3$  recovers to similar values at the end of every winter in both hemispheres, Santee et al. [1999] concluded that the effects of severe denitrification are confined in both space and time to the regions poleward of  $65^\circ\text{S}$  during austral winter and early spring. The EqL averages shown in Figure 4, and those at other  $\theta$  levels, support these conclusions.

The Antarctic daily averages for 1991/1992 and much of 1992/1993 particularly stand out in many EqL bins in Figure 4. For the first few months after the eruption of Mount Pinatubo in June 1991, the strong Antarctic vortex effectively blocked dispersal of volcanic aerosol into the southern polar regions, but aerosol loading at southern midlatitudes ( $<60^\circ\text{S}$ ) was significantly enhanced up to 30 km by September 1991 [Trepte et al., 1993; Thomason et al., 1997; Bauman et al., 2003]. The MLS data obtained in southern midlatitudes at the beginning of November 1991 indicate  $\text{HNO}_3$  abundances that are well outside the envelope of typical values. At the highest EqLs, however,  $\text{HNO}_3$  mixing ratios are



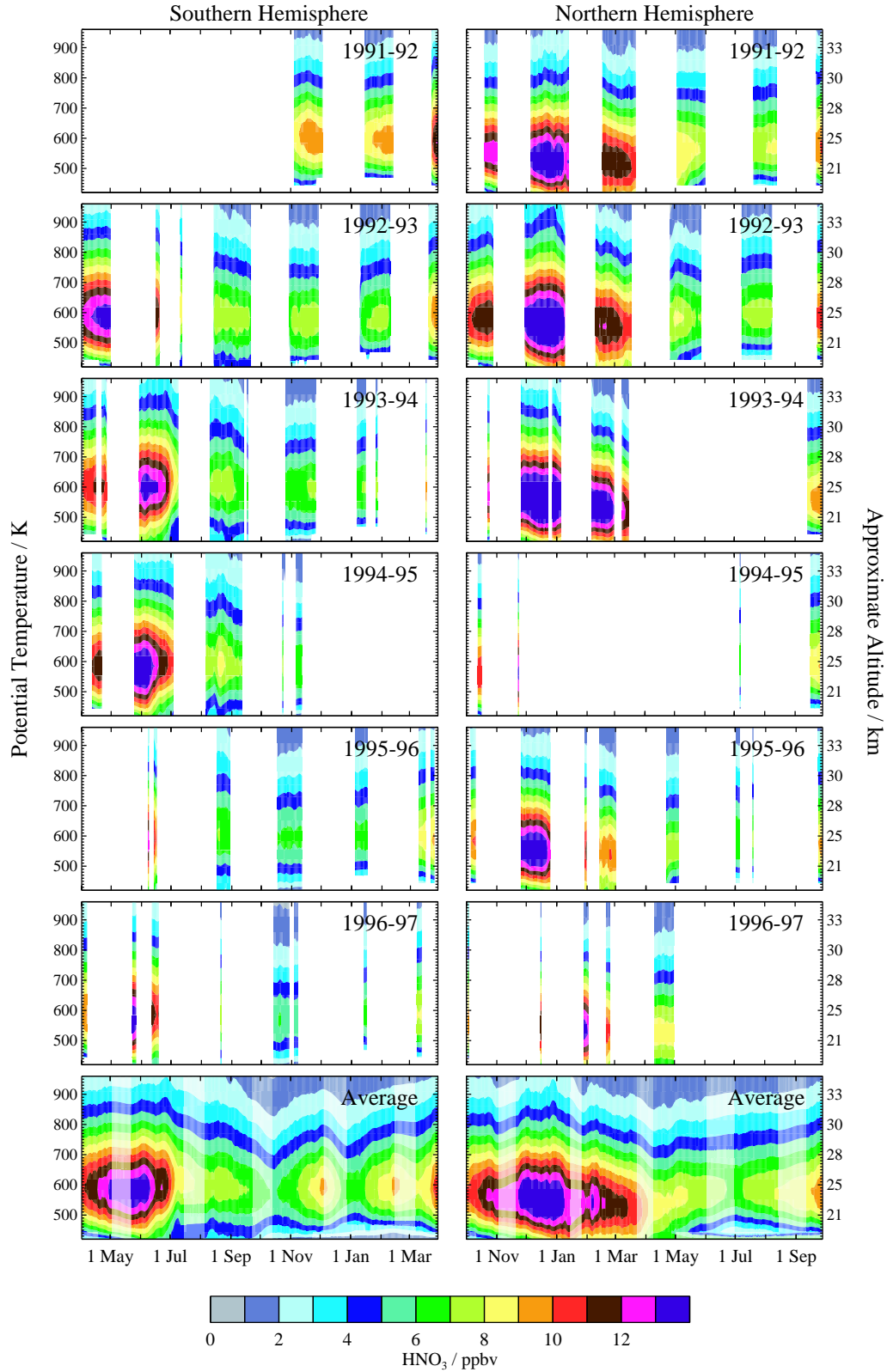


**Figure 3.** Averages of MLS v6  $\text{HNO}_3$  calculated within the 60° EqL contour for the southern (left) and 65° EqL contour for the northern (right) hemispheres as a function of potential temperature from 420 to 960 K. The top six rows show data from individual years; because of decreasing measurement frequency, the data from 1997/1998 have been omitted. Small data gaps in these panels have been filled by running the daily vortex averages through a Kalman smoother. The bottom row shows climatologies derived by averaging together the results for the individual years. As in Figure 2, breaks in the climatological fields have been eliminated by applying a greater degree of Kalman smoothing than was used for the individual years in the panels above; paler colors denote regions where the estimated precision of the interpolated values is poor. The approximate altitude scale is calculated using the nonlinear formula of *Knox* [1998].



not anomalous until mid-November, when they suddenly increase substantially. The timing of this abrupt increase coincides with the breakdown of the polar vortex at this level [Waugh and Randel, 1999; Waugh *et al.*, 1999], allowing a dramatic increase in the aerosol loading at high southern latitudes [e.g., Thomason *et al.*, 1997; Bauman *et al.*, 2003]. The atypically high  $\text{HNO}_3$  concentrations in the southern middle and high latitudes are most likely a consequence of perturbations in reactive nitrogen chemistry induced by the injection of volcanic aerosol [e.g., Hofmann and Solomon, 1989; Brasseur and Granier, 1992; Webster *et al.*, 1994; Rinsland *et al.*, 1994]. The aerosol enhancement at the highest southern latitudes was relatively short-lived, however, and had dissipated to a large extent by the beginning of June 1992 [Thomason *et al.*, 1997; Bauman *et al.*, 2003], when MLS  $\text{HNO}_3$  values at the highest EqLs return to more normal values. Mixing ratios in some midlatitude EqL bins remain elevated for several months longer, consistent with residual volcanic aerosol at lower latitudes [e.g., Bauman *et al.*, 2003].

A fairly similar pattern of southern hemisphere Pinatubo-related  $\text{HNO}_3$  enhancement and recovery is observed up to 840 K (not shown), but not at 420 or 465 K, where the intact vortex was still inhibiting massive intrusion of volcanic aerosol in November 1991, resulting in only moderate enhancement in high-EqL  $\text{HNO}_3$  at these levels (not shown). Unlike at 585 K, at these levels lingering aerosol enhancement [e.g., Bauman *et al.*, 2003] continued to affect  $\text{HNO}_3$  abundances slightly at lower EqLs through the beginning of 1993. Interestingly, however, at no time was the influence of the Pinatubo aerosol on MLS  $\text{HNO}_3$  concentrations at 420 and 465 K as substantial as it was at higher altitudes. This may be a result of the fact that at midlatitudes the conversion of  $\text{NO}_2$  to  $\text{HNO}_3$  saturates at relatively low aerosol loadings at lower altitudes, whereas at higher altitudes much larger aerosol surface areas are required for saturation in the partitioning between  $\text{NO}_2$  and  $\text{HNO}_3$  to occur [e.g., Mills *et al.*, 1993]. Alternatively, it may be linked to differences in the availability of  $\text{NO}_2$ . Stratospheric  $\text{NO}_2$  enhancements (abundances over those expected from  $\text{N}_2\text{O}$  oxidation) arising from the production of  $\text{NO}_x$  in the mesosphere through geomagnetic activity followed by descent are fairly regular occurrences [Siskind *et al.*, 1997, 2000; Randall *et al.*, 1998, 2001; Rinsland *et al.*, 1999]. In particular, a layer of enhanced  $\text{NO}_2$  in the southern hemisphere midstratosphere was seen in UARS Halogen Occultation Experiment (HALOE) data in November 1991 [Siskind *et al.*, 2000]. Because of their timing, however, such  $\text{NO}_2$  enhancements typically have little effect on the lower stratosphere as the vortex dissipates before descent can bring air with elevated  $\text{NO}_2$  down to the lowest levels [e.g., Randall *et al.*,

1998].

In contrast to the southern hemisphere,  $\text{HNO}_3$  mixing ratios at 585 K at northern middle and high latitudes were not substantially affected by Pinatubo. Although significant amounts of volcanic aerosol were dispersed poleward during the 1991 boreal autumn at lower altitudes, above  $\sim 24\text{--}25$  km the aerosol enhancement north of  $45\text{--}50^\circ\text{N}$  was relatively moderate and brief [e.g., Thomason *et al.*, 1997; Bauman *et al.*, 2003]. In addition, although the transport of enhanced  $\text{NO}_2$  from the mesosphere is well documented in the Antarctic vortex, there is little or no evidence of anomalously high  $\text{NO}_2$  in the Arctic stratosphere [Siskind *et al.*, 1997; Randall *et al.*, 1998; Rinsland *et al.*, 1999], so there may simply have been less  $\text{NO}_2$  to be converted to  $\text{HNO}_3$  in the north. Kumer *et al.* [1996] also report a distinct decreasing trend in calculated UARS CLAES  $\text{HNO}_3$  column amounts in the southern hemisphere over the period from February 1992 to February 1993, which they attribute to recovery from Pinatubo-related enhancement, but a much weaker decreasing trend in the northern tropics and actually a slight increase in  $\text{HNO}_3$  column amounts over this period at northern middle and high latitudes. Kumer *et al.* [1996] suggest the quasi-biennial oscillation (QBO) as a plausible mechanism for inducing the apparent hemispheric asymmetry in the CLAES  $\text{HNO}_3$  trends during this period.

### 3.2. Seasonal Snapshots

We focus in this section on defining the typical behavior of  $\text{HNO}_3$  during several intervals of particular interest in the annual cycle. As shown by Santée *et al.* [1999] and seen also in the previous figures,  $\text{HNO}_3$  mixing ratios are uniformly low throughout the summer hemisphere and exhibit little day-to-day, interannual, or interhemispheric variability; therefore, the summertime  $\text{HNO}_3$  distribution is not considered further here. Climatological  $\text{HNO}_3$  fields representative of four “seasons” (fall, early winter, late winter, spring) in each hemisphere are produced by averaging together all the data obtained within a 5-day interval on either side of the dates given in Table 1 over a period of seven years. The central dates for these intervals are chosen to maximize data coverage, taking into account missing data and the UARS yaw state, while still allowing comparison of equivalent seasons in the two hemispheres. For any individual year the minimum number of days contributing to the seasonal averages is 2 and the maximum is 11; data from 5–7 individual years, for a total of 34–51 days, are combined for each of the overall seasonal averages. The length of the intervals is limited to 11 days because meteorological conditions, and hence the  $\text{HNO}_3$  distribution, can change rapidly, especially during spring and fall. Similarly, significant changes in high-latitude  $\text{HNO}_3$  abundances over the course of the winter dic-

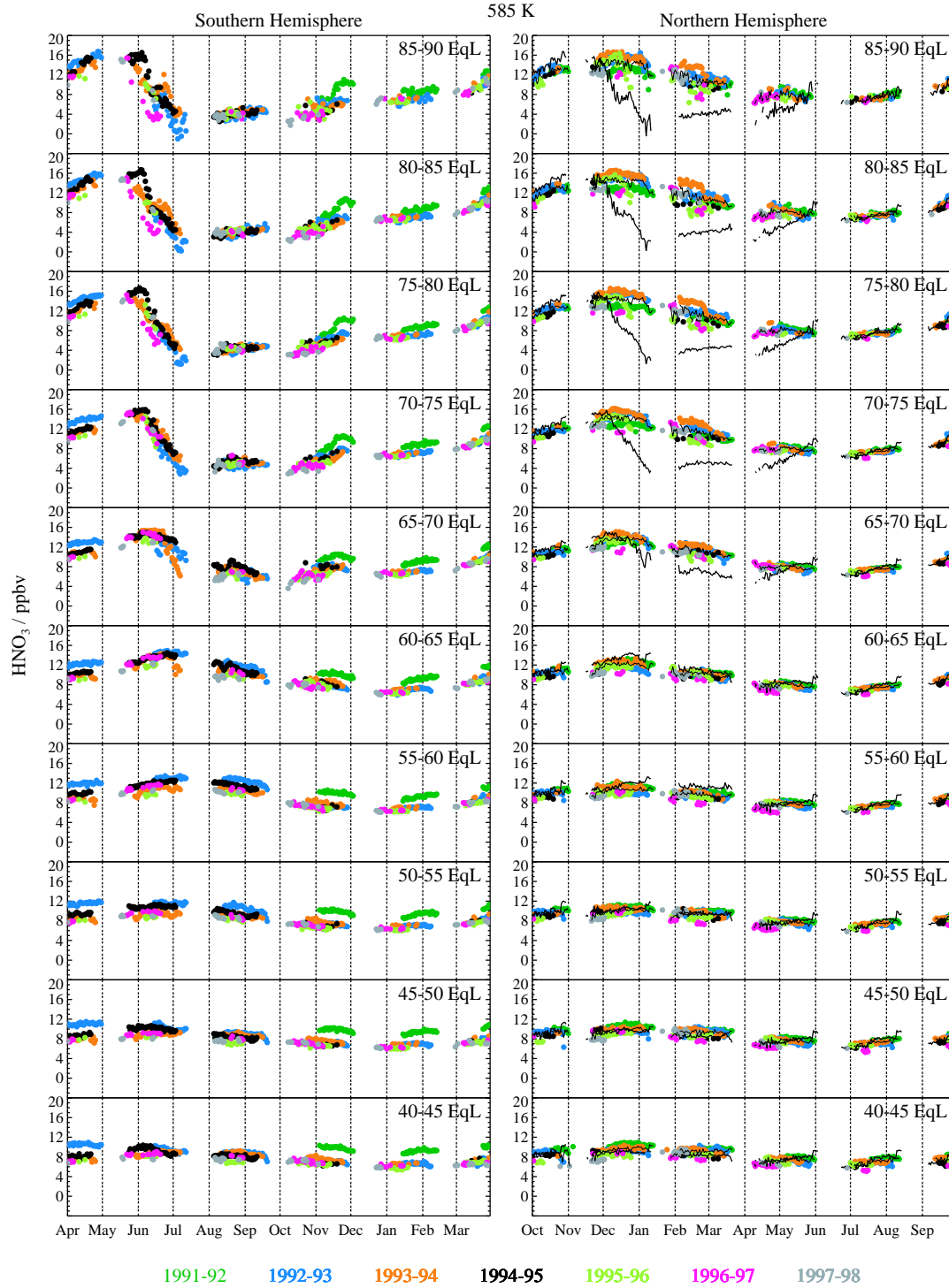


**Figure 4.** Time series of MLS v6  $\text{HNO}_3$  at 585 K for both the southern (left) and northern (right) hemispheres. Measurements were binned into  $5^\circ$  EqL bands and averaged; different years are represented by different colors as indicated in the legend. Dotted vertical lines demark calendar months. Daily averages calculated from the southern hemisphere data points in every year are overlaid on the northern hemisphere plot as a thick black line (shifted by 6 months so that comparable seasons are aligned). To facilitate comparison, the daily averages calculated from the northern hemisphere data points are also overlaid on the northern hemisphere plot as a thin black line.

tate the division of this season into two separate periods. In addition to averaging together the MLS  $\text{HNO}_3$  data for these days, we also average the PV fields from the Met Office analyses. Two contours of PV are overlaid on these plots to illustrate the typical size, shape, and strength of the polar vortex at each level and in each season.

The vertical distribution of  $\text{HNO}_3$  during these four seasons is illustrated in the equivalent latitude/potential temperature ( $\text{EqL}/\theta$ ) representations of Figures 5 and 6.  $\text{HNO}_3$  exhibits little vertical, seasonal, or interannual variability in the tropics. The peak in the vertical profile occurs around 700–750 K near the equator and moves steadily down in altitude to about 550 K in the vortex core in midwinter, as first noted in LIMS data [Gille and Russell, 1984; Gille et al., 1984]. Just inside the vortex edge, the latitudinal gradients are very strong, especially near the profile peak at  $\sim 600$  K; the vertical gradients in this region are also very strong. The pronounced dip in the  $\text{HNO}_3$  contours along the vortex edge is a signature of strong descent. That the peak in the  $\text{HNO}_3$  profile typically occurs at slightly lower altitudes in the northern hemisphere is most likely a consequence of stronger descent there than in the southern hemisphere [e.g., Manney et al., 1994]. A similar pattern of  $\text{HNO}_3$  isopleths that slope downward and poleward in the lower stratosphere but that are relatively flat in the middle stratosphere was also reported in LIMS [Austin et al., 1986] and ATMOS [Manney et al., 1999] measurements.

A striking degree of interannual variability in the seasonal buildup and depletion of  $\text{HNO}_3$  occurs in both hemispheres. One caveat in interpreting these plots is that the gridding and averaging procedures smear out highly localized and transient phenomena such as PSC events; this problem is particularly acute in the Arctic, where PSCs are typically much less extensive and shorter-lived. The late-February intervals in 1996 and 1997, however, were periods of extreme cold with fairly large pockets of substantially depleted  $\text{HNO}_3$  [Santee et al., 1996, 1997]. In fact, 20 February 1996 proved to be the coldest Arctic winter day in the entire UARS MLS data record, with the most Antarctic-like  $\text{HNO}_3$  distribution. The 1996 low- $\text{HNO}_3$  region is not as apparent in these plots because the PSC episode was relatively transitory and about twice as many days as in 1997 contributed to the average in 1996. Compared with the northern hemisphere, the southern hemisphere displays as much (and perhaps even more) interannual variation in the maximum mixing ratios attained in fall and early winter and the spatial extent over which the largest abundances are found. Similarly, although severe  $\text{HNO}_3$  loss is observed at high  $\text{EqL}$ s throughout much of the vertical range every year, the horizontal and vertical extent and the degree of depletion are also highly variable from year to year in the south.

Finally, we present in Figure 7 a set of maps showing climatological  $\text{HNO}_3$  fields for the four seasons in each hemisphere at three potential temperatures. Only the overall averages taken over the seven years of data are shown. Looking first at the fall maps, although in some years  $\text{HNO}_3$  mixing ratios are roughly equal in the two hemispheres (not shown), in the overall climatologies they are slightly larger in the south than in the north at all three levels. As indicated in the time series plots in the previous section, substantial enhancement of  $\text{HNO}_3$  is just starting at this time, as the conversion of  $\text{N}_2\text{O}_5$  proceeds in darkness. The vortex has not yet developed at 465 K in the northern hemisphere, so that any air with higher  $\text{HNO}_3$  brought down from above becomes diluted through mixing with lower-latitude air. At 585 K, the spacing of the PV contours implies a much stronger barrier to mixing in the southern hemisphere, with the effects of confined descent leading to correspondingly larger  $\text{HNO}_3$  values there than in the north. In the midstratosphere, the Arctic vortex on 1 October is approximately the same size and shape as the Antarctic vortex on 1 April [Manney and Zurek, 1993]. Nevertheless,  $\text{HNO}_3$  mixing ratios that are, on average, larger suggest the occurrence of less mixing with extra-vortex air in the south even at this level, despite the fact that the climatological PV contours do not appear significantly different in the two hemispheres. Alternatively, more  $\text{NO}_2$  may have been available for conversion in the south, as suggested earlier. On the other hand, there is a much greater degree of variability, both interannual and day-to-day, in the shape and position of the vortex in the north, particularly in early winter [O'Neill and Pope, 1990; Waugh and Randel, 1999]. Unlike the values shown in all previous plots, which were calculated over  $\text{EqL}$  and thus accounted for differences in vortex shape and position on the days being averaged, the averages of gridded fields displayed in these maps may reflect merged contributions from both vortex and extra-vortex air, even in regions situated within the climatological PV contours designating the vortex edge.

Climatological  $\text{HNO}_3$  values increase between fall and early winter at all levels in both hemispheres. Examination of maps for individual years (not shown), however, reveals that, while a substantial increase occurs in the Arctic in some years (e.g., 1992), little or no increase occurs in others (e.g., 1995, 1996); a similar degree of interannual variability in the seasonal buildup of  $\text{HNO}_3$  is seen in the Antarctic. These results underscore the extent to which a single year can influence climatological fields. Stronger descent in the Arctic leads to mixing ratios that are smaller at 740 K (above the profile peak) but larger at 465 K (below the peak) than in the Antarctic. In addition, the effects of  $\text{HNO}_3$  sequestration in PSCs are already apparent in the Antarctic early winter maps at all three levels, particularly in the area between the

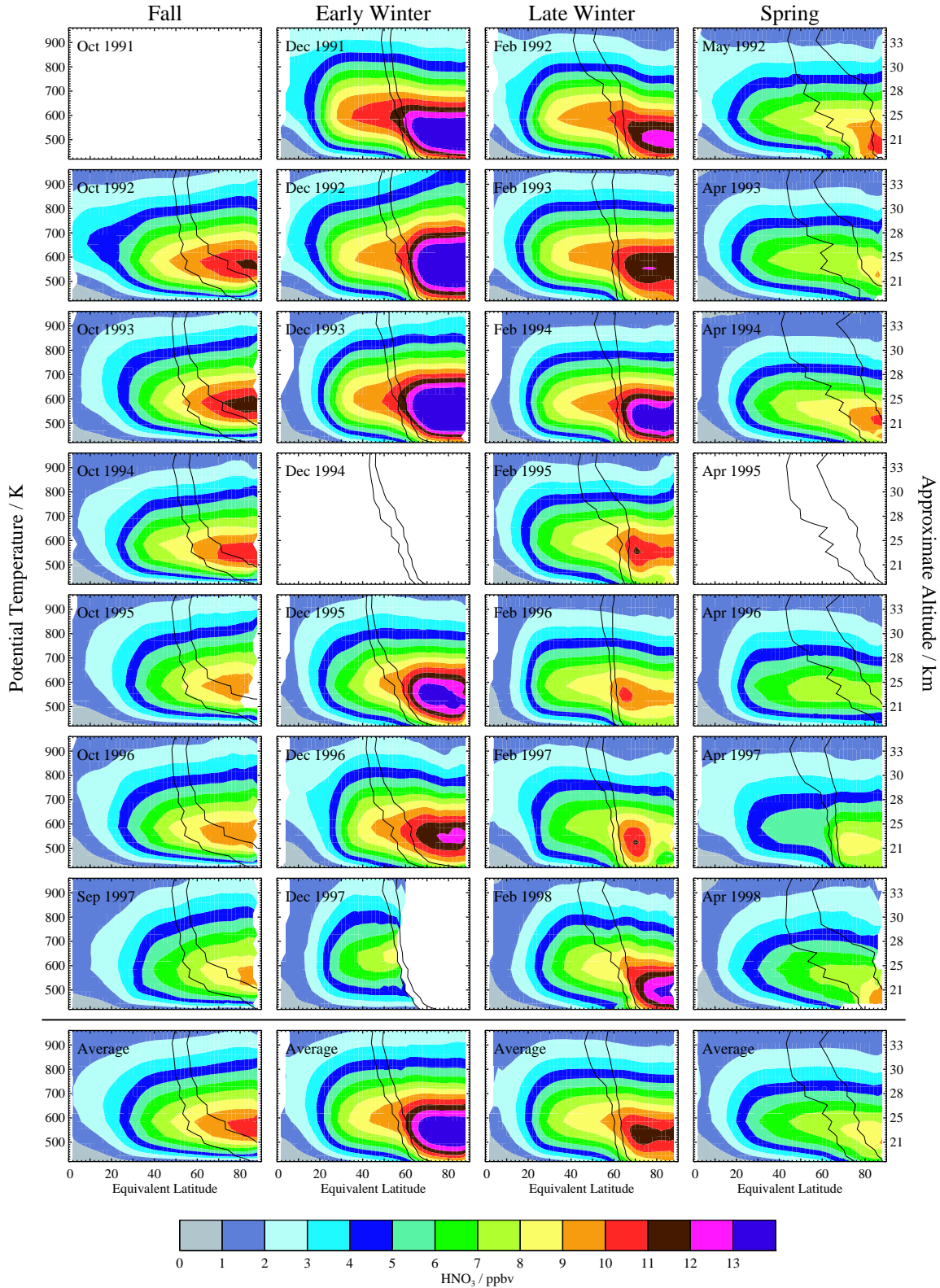


**Figure 5.** Equivalent latitude/potential temperature (EqL/θ) cross sections of MLS v6  $\text{HNO}_3$  in the northern hemisphere averaged over 11-day intervals in four “seasons” in each of seven years (top seven rows). The bottom row shows climatologies derived by averaging together the results for the individual years; they represent averages over a total of 34–51 days, depending on the season (see text). The black lines represent two contours of Met Office potential vorticity (PV), scaled to give similar values throughout the θ domain.

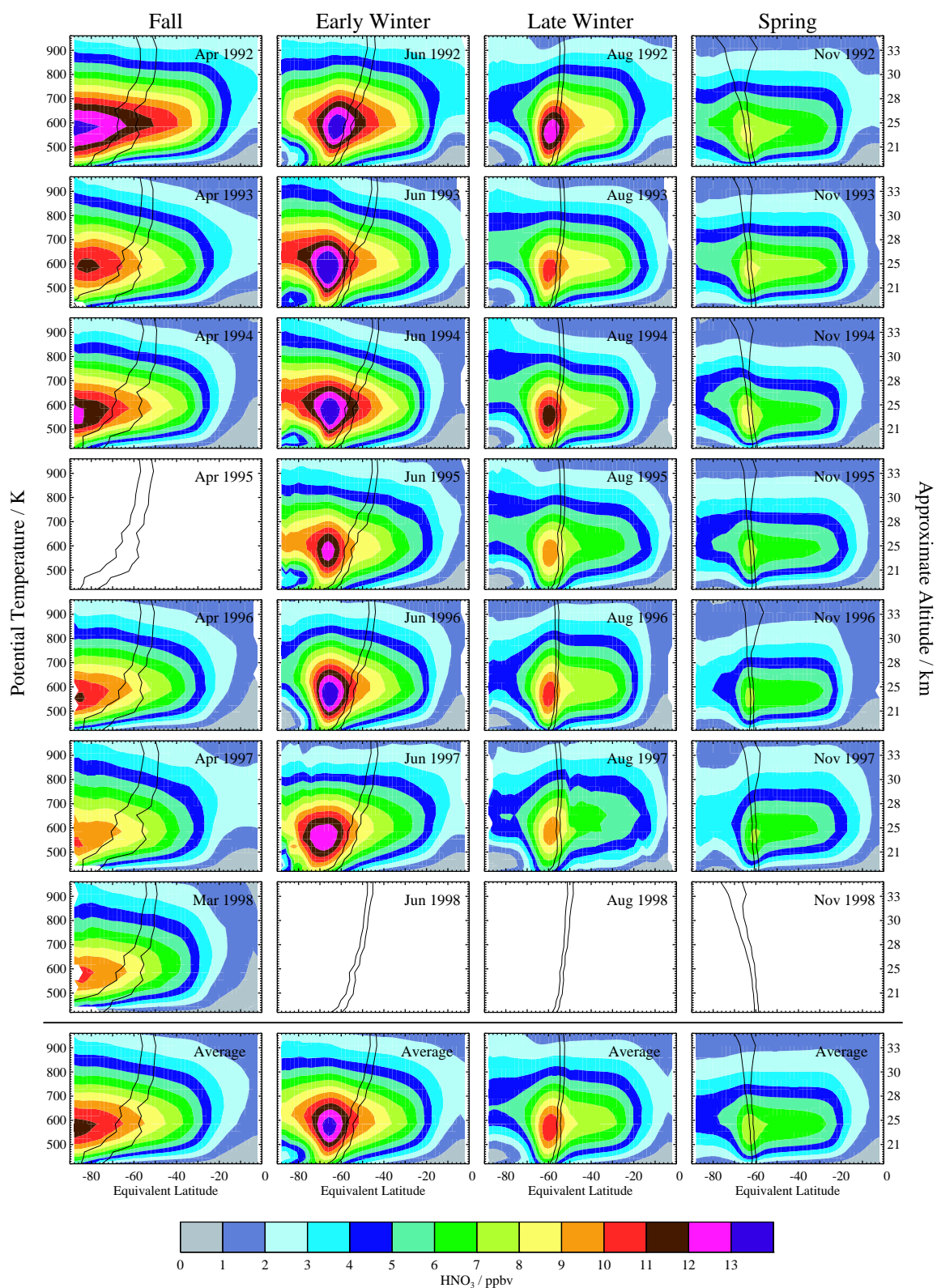


Figure 6. As in Figure 5, for the southern hemisphere.

**Table 1.** Representative Days for Each Season

Hemisphere	Fall	Early Winter	Late Winter	Spring
North	October 1	20 December	25 February	30 April
South	April 1	15 June	25 August	4 November

Palmer Peninsula and the Greenwich Meridian, a region in which PSCs have been shown to form preferentially [Watterson and Tuck, 1989; Poole and Pitts, 1994; Fromm *et al.*, 1997].

By late winter the signature of severe denitrification is apparent over much of the Antarctic vortex up to (and even above, not shown) 740 K. Extensive and persistent PSC formation reduces HNO<sub>3</sub> throughout the lower stratospheric vortex, including (to a lesser extent than in the vortex core) the collar region. In addition, a small degree of intra-vortex mixing with the severely denitrified core may also diminish HNO<sub>3</sub> concentrations near the vortex edge in some years. In contrast, the late winter HNO<sub>3</sub> distribution in the Arctic shows no suggestion of substantial denitrification at any level, although the climatology at 465 K does exhibit slightly depressed HNO<sub>3</sub> concentrations in the preferred PSC formation region between Greenland and Scandinavia. Unlike at 585 and 740 K, where descent acts to reduce HNO<sub>3</sub> mixing ratios from their early winter values throughout the vortex (compare the tilt in the contours in Figure 3), at 465 K descent should continue to increase HNO<sub>3</sub> through the winter. That 465 K abundances have declined slightly in late winter implies that the effects of ongoing sequestration in PSCs and/or denitrification are substantial enough to counteract replenishment by descent even in the northern hemisphere. Indeed, maps for individual years (not shown) indicate no significant decrease between early and late winter in the Arctic in 1993/1994 and 1997/1998, fairly warm years with little midwinter PSC activity, but considerable decreases in 1991/1992, 1992/1993, 1995/1996, and 1996/1997, years with very cold intervals between late December and late February. Significant variability in late winter vortex size, shape, and strength may also affect the climatological maps, as discussed above.

In the spring, the initiation of photolysis with returning sunlight reduces HNO<sub>3</sub> at all levels. The polar vortex erodes from the top down and typically dissipates in the lower stratosphere in late March or early April in the Arctic, whereas it typically remains robust in the lower stratosphere through early to mid-December in the Antarctic [Waugh and Randel, 1999; Waugh *et al.*, 1999]. In the northern hemi-

sphere, the vortex stayed intact throughout the middle and lower stratosphere into early May in 1997 [Coy *et al.*, 1997], and small vortex fragments maintained their identity in late April at least at 465 K in a few other years (e.g., 1992, 1998); HNO<sub>3</sub> enhancement persisted within these vortex remnants (not shown). In other years, however, the breakdown of the vortex led to rapid mixing with low-HNO<sub>3</sub> air by this time.

The enduring depression in HNO<sub>3</sub> abundances in the Antarctic vortex in early November, after stratospheric temperatures have risen well above PSC existence thresholds in every year, confirms that the HNO<sub>3</sub> has been irreversibly removed from these levels through denitrification and is not simply still sequestered in extant PSCs. Indications of denitrification at 740 K show up more clearly in a few individual years (e.g., 1993, 1996, 1997; not shown) but are weakly present in the climatological map. Although low, temperatures at these levels were not below the ice frost point in any of these years. Indeed, inspection of more than 10 years of analyses from the Met Office and more than 20 years of analyses from the National Centers for Environmental Prediction (NCEP) and the NCEP/National Center for Atmospheric Research Reanalysis reveals very little area with temperatures below the frost point at 15 hPa in most years and none at 10 hPa in any year (the 740 K  $\theta$  surface corresponds to pressures of about 10 hPa in the southern hemisphere early/late winter). Consistent with the meteorological conditions, satellite observations from MLS [Stone *et al.*, 2001], HALOE [Rosenlof *et al.*, 1997], and Polar Ozone and Aerosol Measurement (POAM) III [Nedoluha *et al.*, 2000, 2002] have shown that Antarctic dehydration is confined to levels below  $\sim 23$  km ( $\sim 550$  K). On the other hand, the area with temperatures persistently below the existence threshold for nitric acid trihydrate (NAT) PSCs for substantial periods is significant up to and even above 10 hPa in many years (depending on which meteorological analyses are used), and PSCs have occasionally been observed at altitudes as high as 28 km in early and midwinter [Poole and Pitts, 1994; Fromm *et al.*, 1997]. Based on UARS MLS and CLAES measurements, Tabazadeh *et al.* [2000] argued that extensive denitrification precedes significant dehydration by a few weeks at 450 K in the Antarctic. The MLS HNO<sub>3</sub> data



shown here imply that denitrification is an independent process that occurs in the absence of dehydration in the upper portions of the Antarctic lower stratosphere as well. Because of the relatively poor vertical resolution of the MLS  $\text{HNO}_3$  data at this level, however, the values at 655 or even 585 K may have a nonnegligible influence on the 740 K distribution, so that caution must be exercised in interpreting these maps. Nevertheless, the MLS data shown here provide further evidence that the processes of denitrification and dehydration are not strongly coupled.

#### 4. Summary and Conclusions

UARS MLS version 6  $\text{HNO}_3$  measurements were presented to provide an overview of the seasonal, interhemispheric, and interannual variations in the distribution of  $\text{HNO}_3$  over seven annual cycles in the 1990s in both hemispheres throughout the lower and middle stratosphere from 420 to 960 K. Time series of different slices through the data were used to develop a comprehensive picture of the mean evolution of stratospheric  $\text{HNO}_3$  during the UARS timeframe. Maps and equivalent latitude/potential temperature cross sections were shown to illustrate the typical behavior of  $\text{HNO}_3$  during intervals of interest in the annual cycle. Climatological fields were derived by averaging together the results for individual years.

$\text{HNO}_3$  exhibits little vertical, seasonal, or interannual variability in the tropics. For the first  $\sim 1.5$  years of the mission, however, a persistent enhancement is seen, especially at low and midlatitudes, which we attribute to the heterogeneous conversion of  $\text{N}_2\text{O}_5$  under conditions of high aerosol loading from the eruption of Mount Pinatubo. In particular, in the middle stratosphere and the upper portions of the lower stratosphere the MLS data obtained at southern midlatitudes at the beginning of November 1991 indicate  $\text{HNO}_3$  abundances that are well outside the envelope of typical values.  $\text{HNO}_3$  mixing ratios are not anomalous at the highest EqLs until mid-November, when the breakdown of the Antarctic vortex at these levels allows volcanic aerosol to penetrate to high latitudes. At the highest southern latitudes, aerosol enhancement at these levels largely dissipates and MLS  $\text{HNO}_3$  values relax to unperturbed values by the beginning of June 1992, whereas at some midlatitude EqLs residual volcanic aerosol keeps mixing ratios elevated for several months longer. At the lowest levels (420 and 465 K), lingering aerosol enhancement continues to affect  $\text{HNO}_3$  abundances slightly at lower EqLs through the beginning of 1993. At no time, however, is the influence of the Pinatubo aerosol on MLS  $\text{HNO}_3$  concentrations as dramatic at these levels as it is at higher altitudes. In contrast to the southern hemisphere,  $\text{HNO}_3$  mixing ratios at northern middle and high latitudes

are not substantially affected by Pinatubo.

$\text{HNO}_3$  abundances increase from low to high EqLs in both hemispheres at all levels and in all seasons, with the exception of the severely-denitrified region inside the Antarctic vortex. A pronounced seasonal cycle is present at middle and high EqLs in both hemispheres up to at least 960 K ( $\sim 34$  km), with a winter maximum and a summer minimum. Large interannual variability in the timing, magnitude, and duration of enhanced wintertime  $\text{HNO}_3$  abundances is seen in both hemispheres, and the variability increases with increasing EqL. The peak in the vertical profile occurs around 700–750 K near the equator and moves steadily down in altitude to about 550 K in the vortex core in midwinter. Vortex mixing ratios near the peak are comparable in the two hemispheres. Above the peak maximum abundances are larger in the Antarctic than in the Arctic, whereas below the peak maximum abundances are larger in the north. Maximum abundances are reached at all levels in the north in midwinter (December or early January), whereas PSC formation and denitrification start to reverse the seasonal increase in  $\text{HNO}_3$  abundances in the south in early winter (May). Virtually complete removal of gas-phase  $\text{HNO}_3$  occurs at the highest southern EqLs by July in every year throughout the lower stratosphere. In contrast, even in the coldest Arctic winters  $\text{HNO}_3$  depletion is modest and is also more limited in both horizontal and vertical extent. The slight decline in climatological abundances at the lowest levels between early and late winter, however, implies that, at least in some winters, ongoing sequestration in PSCs and/or denitrification are substantial enough to counteract replenishment by descent even in the northern hemisphere.

The enduring depression in  $\text{HNO}_3$  abundances throughout the still-intact Antarctic lower stratospheric vortex in early November, after stratospheric temperatures have risen well above PSC existence thresholds in every year, confirms that  $\text{HNO}_3$  has been irreversibly removed from these levels through denitrification and is not simply still sequestered in extant PSCs. The EqL averages throughout the lower stratosphere shown here support the conclusions of Santee *et al.* [1999] that the effects of severe denitrification are confined in both space and time to the regions poleward of  $65^\circ\text{S}$  during austral winter and early spring. Indications of denitrification are present up to at least 740 K, well above the highest altitude at which dehydration is observed. Although the signature of denitrification at the top levels may partially arise from lower in the stratosphere (because of the relatively poor vertical resolution of the data at these levels), the MLS  $\text{HNO}_3$  measurements shown here provide further evidence that denitrification can proceed in the absence of dehydration.



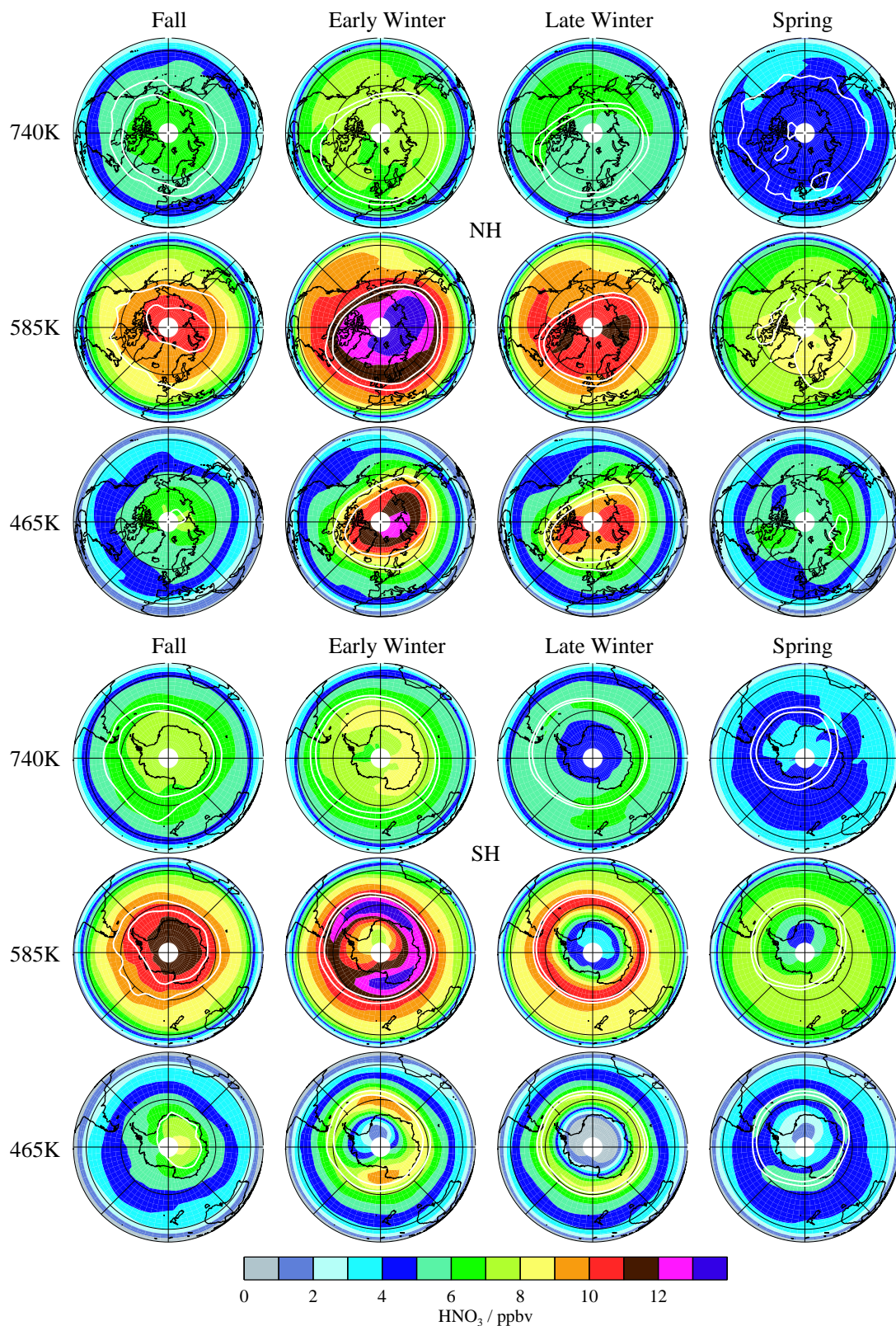


**Figure 7.** Climatological maps of MLS v6  $\text{HNO}_3$  in the northern (top three rows) and southern (bottom three rows) hemispheres for four “seasons” (see Table 1) at 740, 585, and 465 K. Two contours of Met Office PV are overlaid in white on each map to indicate the approximate size and strength of the polar vortex.

## 5. HNO<sub>3</sub> Measurements from Aura MLS

A second-generation MLS experiment is scheduled for launch as part of NASA's EOS Aura mission in 2004. The capability of the Aura MLS instrument, which has a design lifetime of 5 years (vs. 18 months for UARS MLS), is greatly enhanced over that of its predecessor. Three radiometers (at 190, 240, and 640 GHz) will measure HNO<sub>3</sub>. Retrievals using simulated radiances indicate that, compared with the UARS MLS data shown here, Aura MLS HNO<sub>3</sub> measurements will have better vertical resolution ( $\sim 3$  km, vs.  $\sim 6$  km for UARS MLS in the lower stratosphere) over a larger vertical range (215–3.2 hPa vs. 100–4.6 hPa) with similar precision ( $\sim 1.0$ – $1.5$  ppbv over most of the profile). The horizontal resolution will also be better:  $\sim 200$ – $300$  km along-track and  $\sim 3$ – $9$  km across-track (vs.  $\sim 400$  km  $\times$   $400$  km for UARS MLS). The simulation results suggest that average biases are expected to be small at most latitudes and altitudes, with the overall accuracy better than 10% from 147 to 4.6 hPa. Perhaps most importantly, Aura MLS will perform measurements with the instrument fields of view scanning the limb in the orbit plane to provide latitudinal coverage that extends from 82°N to 82°S on every orbit, affording continuous monitoring of the polar regions (no monthly gaps arising from yaw maneuvers as on UARS). Daily global coverage will greatly facilitate the derivation of climatologies such as the ones shown here, and the improved vertical and horizontal resolution of the data will enhance the usefulness of climatological fields.

**Acknowledgments.** We thank C. Randall for very helpful comments and the U.K. Met Office (especially R. Swinbank) for meteorological analyses. Work at the Jet Propulsion Laboratory, California Institute of Technology, was done under contract with the National Aeronautics and Space Administration.

## References

- Andrews, D. G., Some comparisons between the middle atmosphere dynamics for the southern and northern hemispheres, *Pure Appl. Geophys.*, **130**, 213–232, 1989.
- Austin, J., R. R. Garcia, J. M. Russell, S. Solomon, and A. F. Tuck, On the atmospheric photochemistry of nitric acid, *J. Geophys. Res.*, **91**, 5477–5485, 1986.
- Barath, F. T., et al., The Upper Atmosphere Research Satellite Microwave Limb Sounder Instrument, *J. Geophys. Res.*, **98**, 10,751–10,762, 1993.
- Bauman, J. J., P. B. Russell, M. A. Geller, and P. Hamill, A stratospheric aerosol climatology from SAGE II and CLAES measurements: 2. results and comparisons, 1984–1999, *J. Geophys. Res.*, **108**, 4383, doi:10.1029/2002JD002993, 2003.
- Bowman, K. P., Large-scale isentropic mixing properties of the Antarctic polar vortex from analyzed winds, *J. Geophys. Res.*, **98**, 23,013–23,027, 1993.
- Brasseur, G., and C. Granier, Mount Pinatubo aerosols, chlorofluorocarbons, and ozone depletion, *Science*, **257**, 1239–1242, 1992.
- Butchart, N., and E. E. Remsberg, The area of the stratospheric polar vortex as a diagnostic for tracer transport on an isentropic surface, *J. Atmos. Sci.*, **43**, 1319–1339, 1986.
- Coy, L., E. R. Nash, and P. A. Newman, Meteorology of the polar vortex: Spring 1997, *Geophys. Res. Lett.*, **24**, 2693–2696, 1997.
- Danilin, M. Y., et al., Trajectory hunting as an effective technique to validate multiplatform measurements: Analysis of the MLS, HALOE, SAGE-II, ILAS, and POAM-II data in October–November 1996, *J. Geophys. Res.*, **107**, 10.1029/2001JD002012, 2002.
- David, S. J., F. J. Murcray, A. Goldman, C. P. Rinsland, and D. G. Murcray, The effect of the Mt. Pinatubo aerosol on the HNO<sub>3</sub> column over Mauna Loa, Hawaii, *Geophys. Res. Lett.*, **21**, 1003–1006, 1994.
- de Zafra, R. L., and S. P. Smyshlyaev, On the formation of HNO<sub>3</sub> in the Antarctic mid to upper stratosphere in winter, *J. Geophys. Res.*, **106**, 23,115–23,125, 2001.
- de Zafra, R. L., V. Chan, S. Crewell, C. Trimble, and J. M. Reeves, Millimeter wave spectroscopic measurements over the South Pole, 3, The behavior of stratospheric nitric acid through polar fall, winter, and spring, *J. Geophys. Res.*, **102**, 1399–1410, 1997.
- de Zafra, R. L., G. Muscari, and S. P. Smyshlyaev, On the cryogenic removal of NO<sub>y</sub> from the Antarctic polar stratosphere, *Ann. Geophys.*, **46**, 285–294, 2003.
- Fromm, M. D., J. D. Lumpe, R. M. Bevilacqua, E. P. Shettle, J. Hornstein, S. T. Massie, and K. H. Fricke, Observations of Antarctic polar stratospheric clouds by POAM II: 1994–1996, *J. Geophys. Res.*, **102**, 23,659–23,672, 1997.
- Fromm, M. D., R. M. Bevilacqua, J. Hornstein, E. P. Shettle, K. Hoppel, and J. D. Lumpe, An analysis of Polar Ozone and Aerosol Measurement POAM II Arctic stratospheric cloud observations, 1993–1996, *J. Geophys. Res.*, **104**, 24,341–24,357, 1999.
- Gille, J. C., and J. M. Russell, The Limb Infrared Monitor of the Stratosphere: Experiment description, performance, and results, *J. Geophys. Res.*, **89**, 5125–5140, 1984.
- Gille, J. C., et al., Accuracy and precision of the nitric acid concentrations determined by the Limb Infrared Monitor of the Stratosphere experiment on NIMBUS 7, *J. Geophys. Res.*, **89**, 5179–5190, 1984.
- Hofmann, D. J., and S. Solomon, Ozone destruction through heterogeneous chemistry following the eruption of El Chichón, *J. Geophys. Res.*, **94**, 5029–5041, 1989.
- Kawa, S. R., J. B. Kumer, A. R. Douglass, A. E. Roche, S. E. Smith, F. W. Taylor, and D. J. Allen, Missing chemistry of reactive nitrogen in the upper stratospheric polar winter, *Geophys. Res. Lett.*, **22**, 2629–2632, 1995.
- Knox, J. A., On converting potential temperature to altitude in the middle atmosphere, *Eos Trans. AGU*, **79**, 376, 1998.
- Koike, M., N. B. Jones, W. A. Matthews, P. V. Johnston, R. L. McKenzie, D. Kinnison, and J. Rodriguez, Impact of Pinatubo aerosols on the partitioning between NO<sub>2</sub> and HNO<sub>3</sub>, *Geophys. Res. Lett.*, **21**, 597–600, 1994.

- Kumer, J. B., et al., Comparison of correlative data with  $\text{HNO}_3$  version 7 from the CLAES instrument deployed on the NASA Upper Atmosphere Research Satellite, *J. Geophys. Res.*, **101**, 9621–9656, 1996.
- Lee, A. M., H. K. Roscoe, A. E. Jones, P. H. Haynes, E. F. Shuckburgh, M. W. Morrey, and H. C. Pumphrey, The impact of the mixing properties within the Antarctic stratospheric vortex on ozone loss in spring, *J. Geophys. Res.*, **106**, 3203–3211, 2001.
- Livesey, N. J., et al., The UARS Microwave Limb Sounder version 5 dataset: Theory, characterization and validation.
- Manney, G. L., and R. W. Zurek, Interhemispheric comparison of the development of the stratospheric polar vortex during fall: A 3-dimensional perspective for 1991–92, *Geophys. Res. Lett.*, **20**, 1275–1278, 1993.
- Manney, G. L., R. W. Zurek, A. O'Neill, and R. Swinbank, On the motion of air through the stratospheric polar vortex, *J. Atmos. Sci.*, **51**, 2973–2994, 1994.
- Manney, G. L., H. A. Michelsen, M. L. Santee, M. R. Gunson, F. W. Irion, A. E. Roche, and N. J. Livesey, Polar vortex dynamics during spring and fall diagnosed using trace gas observations from the Atmospheric Trace Molecule Spectroscopy instrument, *J. Geophys. Res.*, **104**, 18,841–18,866, 1999.
- McDonald, M., R. L. de Zafra, and G. Muscari, Millimeter wave spectroscopic measurements over the South Pole, 5. Morphology and evolution of  $\text{HNO}_3$  vertical distribution, 1993 versus 1995, *J. Geophys. Res.*, **105**, 17,739–17,750, 2000.
- Mills, M. J., A. O. Langford, T. J. O'Leary, K. Arpag, H. L. Miller, M. H. Proffitt, R. W. Sanders, and S. Solomon, On the relationship between stratospheric aerosols and nitrogen dioxide, *Geophys. Res. Lett.*, **20**, 1187–1190, 1993.
- Mills, M. J., O. B. Toon, and S. Solomon, A 2D microphysical model of the polar stratospheric CN layer, *Geophys. Res. Lett.*, **26**, 1133–1136, 1999.
- Muscari, G., M. L. Santee, and R. L. de Zafra, Intercomparison of stratospheric  $\text{HNO}_3$  measurements over Antarctica: Ground-based Millimeter-wave versus UARS/MLS Version 5 retrievals, *J. Geophys. Res.*, **107**, 4809, doi:10.1029/2002JD002546, 2002.
- Nedoluha, G. E., R. M. Bevilacqua, K. W. Hoppel, M. Daehler, E. P. Shettle, J. H. Hornstein, M. D. Fromm, J. D. Lumpe, and J. E. Rosenfeld, POAM III measurements of dehydration in the Antarctic lower stratosphere, *Geophys. Res. Lett.*, **27**, 1683–1686, 2000.
- Nedoluha, G. E., R. M. Bevilacqua, K. W. Hoppel, J. D. Lumpe, and H. Smit, Polar Ozone and Aerosol Measurement III measurements of water vapor in the upper troposphere and lowermost stratosphere, *J. Geophys. Res.*, **107**, 10.1029/2001JD000793, 2002.
- O'Neill, A., and V. D. Pope, The seasonal evolution of the extra-tropical stratosphere in the southern and northern hemispheres: Systematic changes in potential vorticity and the non-conservative effects of radiation, in *Dynamics, Transport and Photochemistry in the Middle Atmosphere of the Southern Hemisphere*, edited by A. O'Neill, pp. 33–54, Kluwer Acad., Norwell, Mass., 1990.
- Pawson, S., and B. Naujokat, The cold winters of the middle 1990s in the northern lower stratosphere, *J. Geophys. Res.*, **104**, 14,209–14,222, 1999.
- Poole, L. R., and M. C. Pitts, Polar stratospheric cloud climatology based on Stratospheric Aerosol Measurement II observations from 1978 to 1989, *J. Geophys. Res.*, **99**, 13,083–13,089, 1994.
- Randall, C. E., D. W. Rusch, R. M. Bevilacqua, K. W. Hoppel, and J. D. Lumpe, Polar Ozone and Aerosol Measurement (POAM) II stratospheric  $\text{NO}_2$ , 1993–1996, *J. Geophys. Res.*, **103**, 28,361–28,371, 1998.
- Randall, C. E., R. M. Bevilacqua, J. D. Lumpe, and K. W. Hoppel, Validation of POAM III aerosols: Comparison to SAGE II and HALOE, *J. Geophys. Res.*, **106**, 27,525–27,536, 2001.
- Randel, W. J., F. Wu, J. M. Russell, and J. W. Waters, Space-time patterns of trends in stratospheric constituents derived from UARS measurements, *J. Geophys. Res.*, **104**, 3711–3727, 1999.
- Read, W. G., L. Froidevaux, and J. W. Waters, Microwave Limb Sounder (MLS) measurements of  $\text{SO}_2$  from Mt. Pinatubo volcano, *Geophys. Res. Lett.*, **20**, 1299–1302, 1993.
- Rinsland, C. P., D. K. Weisenstein, M. K. W. Ko, C. J. Scott, L. S. Chiou, E. Mahieu, R. Zander, and P. Demoulin, Post-Mount Pinatubo eruption ground-based infrared stratospheric column measurements of  $\text{HNO}_3$ ,  $\text{NO}$ , and  $\text{NO}_2$  and their comparison with model calculations, *J. Geophys. Res.*, **108**, 4437, doi:10.1029/2002JD002965, 2003.
- Rinsland, C. P., et al., Heterogeneous conversion of  $\text{N}_2\text{O}_5$  to  $\text{HNO}_3$  in the post-Mount Pinatubo eruption stratosphere, *J. Geophys. Res.*, **99**, 8213–8219, 1994.
- Rinsland, C. P., et al., Polar stratospheric descent of  $\text{NO}_y$  and CO and Arctic denitrification during winter 1992–1993, *J. Geophys. Res.*, **104**, 1847–1861, 1999.
- Rosenlof, K. H., A. F. Tuck, K. K. Kelly, J. M. Russell, and M. P. McCormick, Hemispheric asymmetries in water vapor and inferences about transport in the lower stratosphere, *J. Geophys. Res.*, **102**, 13,213–13,234, 1997.
- Santee, M. L., W. G. Read, J. W. Waters, L. Froidevaux, G. L. Manney, D. A. Flower, R. F. Jarnot, R. S. Harwood, and G. E. Peckham, Interhemispheric differences in polar stratospheric  $\text{HNO}_3$ ,  $\text{H}_2\text{O}$ ,  $\text{ClO}$ , and  $\text{O}_3$ , *Science*, **267**, 849–852, 1995.
- Santee, M. L., G. L. Manney, W. G. Read, L. Froidevaux, and J. W. Waters, Polar vortex conditions during the 1995–96 Arctic winter: MLS  $\text{ClO}$  and  $\text{HNO}_3$ , *Geophys. Res. Lett.*, **23**, 3207–3210, 1996.
- Santee, M. L., G. L. Manney, L. Froidevaux, R. W. Zurek, and J. W. Waters, MLS observations of  $\text{ClO}$  and  $\text{HNO}_3$  in the 1996–97 Arctic polar vortex, *Geophys. Res. Lett.*, **24**, 2713–2716, 1997.
- Santee, M. L., G. L. Manney, L. Froidevaux, W. G. Read, and J. W. Waters, Six years of UARS Microwave Limb Sounder  $\text{HNO}_3$  observations: Seasonal, interhemispheric, and interannual variations in the lower stratosphere, *J. Geophys. Res.*, **104**, 8225–8246, 1999.
- Schoeberl, M. R., L. R. Lait, P. A. Newman, and J. E. Rosenfeld, The structure of the polar vortex, *J. Geophys. Res.*, **97**, 7859–7882, 1992.
- Siskind, D. E., J. T. Bacmeister, M. E. Summers, and J. M. Russell, Two-dimensional model calculations of nitric oxide transport in the middle atmosphere and comparison with Halogen Occultation Experiment data, *J. Geophys. Res.*, **102**, 3527–3545, 1997.
- Siskind, D. E., G. E. Nedoluha, C. E. Randall, M. Fromm, and J. M. Russell, An assessment of Southern Hemisphere stratospheric

- $\text{NO}_x$  enhancements due to transport from the upper atmosphere, *Geophys. Res. Lett.*, **27**, 329–332, 2000.
- Slusser, J., et al., High-latitude stratospheric  $\text{NO}_2$  and  $\text{HNO}_3$  over Fairbanks ( $65^\circ\text{N}$ ) 1992–1994, *J. Geophys. Res.*, **103**, 1549–1554, 1998.
- Solomon, S., Stratospheric ozone depletion: A review of concepts and history, *Rev. Geophys.*, **37**, 275–316, 1999.
- Stone, E. M., A. Tabazadeh, E. Jensen, H. C. Pumphrey, M. L. Santee, and J. L. Mergenthaler, Onset, extent, and duration of dehydration in the Southern Hemisphere polar vortex, *J. Geophys. Res.*, **106**, 22,979–22,989, 2001.
- Swinbank, R., and A. O'Neill, A stratosphere-troposphere data assimilation system, *Mon. Weather Rev.*, **122**, 686–702, 1994.
- Tabazadeh, A., M. L. Santee, M. Y. Danilin, H. C. Pumphrey, P. A. Newman, P. J. Hamill, and J. L. Mergenthaler, Quantifying denitrification and its effect on ozone recovery, *Science*, **288**, 1407–1411, 2000.
- Thomason, L. W., L. R. Poole, and T. Deshler, A global climatology of stratospheric aerosol surface area density derived from Stratospheric Aerosol and Gas Experiment II measurements: 1984–1994, *J. Geophys. Res.*, **102**, 8967–8976, 1997.
- Toon, G. C., C. B. Farmer, L. L. Lowes, P. W. Schaper, J.-F. Blavier, and R. H. Norton, Infrared aircraft measurements of stratospheric composition over Antarctica during September 1987, *J. Geophys. Res.*, **94**, 16,571–16,596, 1989.
- Trepte, C. R., R. E. Veiga, and M. P. McCormick, The poleward dispersal of Mount Pinatubo volcanic aerosol, *J. Geophys. Res.*, **98**, 18,563–18,573, 1993.
- Waters, J. W., Microwave limb sounding, in *Atmospheric Remote Sensing by Microwave Radiometry*, edited by M. A. Janssen, chap. 8, pp. 383–496, John Wiley, New York, 1993.
- Waters, J. W., et al., The UARS and EOS Microwave Limb Sounder (MLS) experiments, *J. Atmos. Sci.*, **56**, 194–218, 1999.
- Watterson, I. G., and A. F. Tuck, A comparison of the longitudinal distributions of polar stratospheric clouds and temperatures for the 1987 Antarctic spring, *J. Geophys. Res.*, **94**, 16,511–16,525, 1989.
- Waugh, D. W., and W. J. Randel, Climatology of Arctic and Antarctic polar vortices using elliptical diagnostics, *J. Atmos. Sci.*, **56**, 1594–1613, 1999.
- Waugh, D. W., W. J. Randel, S. Pawson, P. A. Newman, and E. R. Nash, Persistence of the lower stratospheric polar vortices, *J. Geophys. Res.*, **104**, 27,191–27,201, 1999.
- Webster, C. R., R. D. May, M. Allen, L. Jaegle, and M. P. McCormick, Balloon profiles of stratospheric  $\text{NO}_2$  and  $\text{HNO}_3$  for testing the heterogeneous hydrolysis of  $\text{N}_2\text{O}_5$  on sulfate aerosols, *Geophys. Res. Lett.*, **21**, 53–56, 1994.
- World Meteorological Organization, *Scientific assessment of ozone depletion: 2002*, Global Ozone Res. and Monit. Proj. Rep. No. 47, Geneva, 2003.
- Zurek, R. W., G. L. Manney, A. J. Miller, M. E. Gelman, and R. M. Nagatani, Interannual variability of the north polar vortex in the lower stratosphere during the UARS mission, *Geophys. Res. Lett.*, **23**, 289–292, 1996.

M. L. Santee (corresponding author), N. J. Livesey, and W. G. Read, Jet Propulsion Laboratory, Mail Stop 183–701, 4800 Oak Grove Drive, Pasadena, CA 91109. (e-mail: mls@mls.jpl.nasa.gov)

G. L. Manney, Department of Natural Sciences, New Mexico Highlands University, Las Vegas, NM 87701.

---

This preprint was prepared with AGU's L<sup>A</sup>T<sub>E</sub>X macros v4, with the extension package 'AGU<sup>++</sup>' by P. W. Daly, version 1.5g from 1998/09/14.